Fibroblasts-dependent maturation and phenotype exacerbation of dystrophic hiPSC-derived MYOtissues enables muscle strength evaluation for gene therapy screening

Short title

DMD MYOtissues as screening platform for gene therapy

Laura Palmieri [1,2], Melissa Moula,[1,2], Abbass Jaber[1,2], Riyad El-Khoury [1,2,3], Guy Brochiet[3,4], Anne Bigot[5], David Israeli [1,2], IsabelleRichard[1,2], Sonia Albini[1,2*]

[1]Genethon, 91100 Evry, France; [2]Université Paris-Saclay, Univ Evry, Inserm, Généthon, Integrare research unit UMR_S951, 91000, Evry, France. [3]Institut de Myologie, Neuromuscular Morphology Unit, Groupe Hospitalier Pitié-Salpêtrière, Paris, France.[4]AP-HP, Centre de Référence de Pathologie Neuromusculaire Nord/Est/Ile de France, Groupe Hospitalier Pitié-Salpêtrière, Paris, France. [5]Sorbonne Université, Inserm, Institut de Myologie, Centre de Recherche en Myologie, F-75013 Paris, France.

[*] Corresponding author. Email: salbini@genethon.fr, ORCID: 0000-0001-9502-1004

ABSTRACT

Duchenne muscular dystrophy (DMD) is a lethal muscle wasting disease caused by absence of dystrophin, a protein essential to preserve muscle integrity continuously challenged by contractions. Gene therapy utilizing adeno-associated virus (AAV) to deliver truncated forms of dystrophin (µDys) is currently the most promising therapeutic approach. However, the therapeutic outcome in treated patients has not been as successful as anticipated by animal studies, underscoring the need of improved and high-throughput models for accurate and fast prediction of human response. Here, we describe the generation of MYOtissues, a 3D muscle platform based on direct myogenic conversion of human induced pluripotent stem cells (iPSC), whose structural and functional maturation is enhanced by fibroblasts incorporation. MYOtissues derived from DMD-iPSC including DMD fibroblasts, exacerbated pathogenic hallmarks such as fibrosis and muscle force loss. As a proof of concept, we showed that AAV-mediated µDys gene transfer improved muscle resistance and membrane stability in DMD-MYOtissues, highlighting the suitability of our system for gene therapy screening.

Introduction

Duchenne muscular dystrophy (DMD; ONIM: #310200) is the most common and severe muscle disorder in children, with a prevalence of 1:5000 boys (1) with no resolutive cure up to date. DMD is caused by genetic mutations in the dystrophin gene that results in the lack of Dystrophin, a key protein of the sarcolemma required for the biochemical support of myofibers and force transmission (2–5). DMD is characterized by progressive muscle wasting affecting skeletal muscles primarily and cardiac and respiratory muscles later, thereby causing premature death (6). Dystrophin links the sarcolemma with the extracellular matrix (ECM) through the dystrophin glycoprotein complex (DGC) and therefore its absence renders muscle cells susceptible to contraction-induced damage (7,8). Moreover, consecutive rounds of muscle membrane degeneration and regeneration caused by the mechanical stress, induce, in turn, secondary pathogenic events such as chronic inflammation and fibrosis that exacerbate the disease phenotype (9–12). Fibrosis, an excessive deposition of ECM components, is a critical driver of DMD progression. Indeed, secretion of TGFβ (Transforming Growth Factor beta), the major profibrogenic factor released from damaged muscle cells, stimulates the production of ECM components, mainly from fibroblasts but also autonomously from myofibers (13–15) causing loss of muscle function.

Gene therapy exploiting adeno-associated virus (AAV) to deliver the therapeutic payload is currently the most promising therapeutical approach for DMD as proved by ongoing clinical trials employing short forms of Dystrophin (µDys) encoding a truncated, but functional, protein (16–22). However, while the therapeutic effects were unequivocally achieved in DMD animal models, the results from clinical trials revealed limited therapeutic efficacy as well as unexpected safety issues (23).

These observations confirm the limited translatability of results obtained in animal models to human patients. Moreover, increasing evidences highlighted the sub-optimal activity of µDys, likely due to absent protein domains, preventing full correction of the phenotype and making necessary the investigation of new treatments (24,25). It appears therefore crucial to develop high throughput models mimicking human DMD pathology, suitable to quickly test the efficacy of therapeutics, more reliably and with reduced animal waste and costs. *In vitro* modeling based on human cells is a valuable option. In particular, the induced pluripotent stem cells (iPSC) technology offers the opportunity to derive an unlimited number of specialized cells using patients' cells for disease modeling and drug screening (26,27). Among the *in vitro* cellular models, organoid-like structures are becoming invaluable for disease modeling as the use of 3D cultures and biomaterials allows the reconstitution of tissue architecture and microenvironment that are instrumental for

pathophysiological evaluations (28,29). However, organoid applications for AAV gene therapy have been limitedly explored and mostly in the context of retinopathies (27,30–34). No reports are available to date on the use of muscle organoids for AAV gene replacement therapy application and only AAV-based CRISPR-Cas9 correction of DMD iPSC prior to formation of organoids were reported as gene therapy approach (35).

For skeletal muscle engineering, several differentiation protocols from human IPSC (iPSC) are available (36–39). However, they present limitations associated with the long duration of the protocol, up to 60 days, due to the multiple cellular transitions mediated by media supplementations. Although this approach mimics muscle development, it is subjected to higher inter-experimental variability due to the heterogeneity of the cell population. Additionally, muscle force analysis remains a challenge in the field, only partially explored, especially for muscle resistance evaluation. Here, we described the rapid generation of iPSC-derived muscle organoid-like structure, crafted to include only specific cell types, and named hereafter MYOtissues. We employed and adapted an engineered muscle platform to generate MYOtissues using a previously reported method for direct iPSC conversion into skeletal muscles cells (13,40,41). We further included fibroblasts to increase structural maturation, according to their reported role in helping muscle assembly, and as a source of microenvironment cues exerted by their secretory activity (42–45). We demonstrated that fibroblasts-including MYOtissues showed improved structural organization and developed higher muscle force during contractions. Remarkably, DMD iPSC-derived MYOtissues that included DMD-fibroblasts displayed exacerbated pathogenic features related to muscle fragility, that allowed significant detection of muscle dysfunctions defined as key therapeutic readouts.

We then applied AAV-mediated µDys gene replacement, a gold standard in DMD gene therapy, as a proof of concept of the suitability of MYOtissues as a platform for therapeutic evaluation. We showed a dose-dependent response in the efficacy of µDys to restore muscle function and membrane stability and revealed partial correction at optimal doses. Our findings indicate that MYOtissues derived from dystrophic iPSC, whose phenotype is exacerbated by fibroblast inclusion, could be used as preclinical human models for muscle force-based screens with the potential to accelerate the identifications of effective therapeutics for DMD.

Results

Generation of structurally organized 3D human MYOtissues by direct conversion of iPSC and inclusion of fibroblasts

MYOtissues were generated from human iPSC committed to differentiate into the myogenic lineage by inducible expression of MyoD and BAF60C (13), from now on referred as iPSC$^{BM.}$. MYOtissues were prepared starting from iPSC^{BM} after one day from the induction of myogenic genes. Casting procedure was performed through adaptation of an engineered muscle system (39,46) which results in the growth of the tissue in a ring format supported by two flexible silicon stretchers (**Figure 1A**). The differentiation protocol was optimized from the conditions previously reported (13,40,41) using myogenic commercial media that ensured the highest expression of myogenic markers and myogenic differentiation in monolayer condition. Since cellular heterogenicity, especially of mesenchymal origin, has been shown to be important for muscle formation (39,45,47,48), we included human immortalized fibroblasts during the casting procedure, to assess whether this would affect muscle organization. For this aim, casting was performed using iPSC^{BM} cells in presence or absence of human fibroblasts. The 3D cultures were kept for 2 days in growth medium, afterwards medium was replaced for differentiation for additional 12 days (**Figure 1A**). A pilot study was conducted to identify the optimal fibroblast concentration required to achieve correct differentiation and high-level organization. We found that inclusion of fibroblasts accelerated the condensation of the muscle rings into a compact structure 0.8 mm long and 1mm thick at day 14 (**Figure 1B**). At that time point, we characterized the muscle differentiation in the MYOtissues by performing immunofluorescence (IF) in whole-mount tissues for sarcomeric α-actinin (SAA), and we could clearly observe an enrichment of SAA positives myotubes throughout the ring-shaped micro-tissue (**Figure 1C**). We then aimed to assess the impact of fibroblasts inclusion on muscle structure. For that, alignment of myotube and circularity were evaluated. Staining for Myosin Heavy Chain (MyHC, myotube marker) and Vimentin (fibroblasts marker) on longitudinal sections showed fibroblasts recruitment near muscle fibers (**Figure 1D**). Measurement of the angles between the myotubes showed a significant decrease with fibroblasts inclusion, which correlates with a better myotube alignment (**Figure 1E**). Additionally, circularity of myofibers was measured from transversal sections stained for the membrane marker WGA (wheat germ agglutinin), using ratio between X and Y Feret diameters (**Figure 1D**). MYOtissues with fibroblasts had an improved circularity (ratio closer to 1) when compared to control (**Figure 1E**). Improved myofiber circularity and myotubes alignment as

shown, indicate that fibroblasts incorporation during the casting procedure, guides myofiber orientation providing structural support for MYOtissues, a prerequisite for maturation.

Improved structural and functional maturation of fibroblast-including MYOtissues

Since muscle function is strictly dependent on the internal myofiber organization, we evaluated the maturation of our 3D MYOtissues by looking at the sarcomere structure. Transversal and longitudinal sections were used to monitor Dystrophin expression at the sarcolemma **(Figure 2A**) and SAA localization for assessment of the striation pattern typical of mature myotubes (**Figure 2B**). Dystrophin was properly localized to the muscle membrane of myotubes from MYOtissues including fibroblasts and was significantly more expressed compared to MYOtissues without fibroblasts (**Figure 2A, D**). Remarkably, the maturation index, reported as percentage of number of nuclei included in striated myotubes, was significantly superior in MYOtissues including fibroblasts as compared to MYOtissues without fibroblasts which appear very disorganized with rare appearance of striations (**Figure 2B, E**). The proper sarcomeric organization was also confirmed by electron microscopy where we could clearly detect longer, properly formed Z patterning, presence of I and A bands along with an overall increase of sarcomeric density and alignment (**Figure 2C**). We further performed gene expression analysis for terminal differentiation markers such as muscle creatine kinase (*MCK*), myosin heavy chain isoforms, such as *MYH2*, representative of fast adult fiber type, and *MYH7*, as a slow fibers marker (**Figure 2F**). Higher expression of all genes in MYOtissues containing fibroblasts, confirms the acquisition of a more mature state, compared to MYOtissues without fibroblasts.

We then assessed whether our MYOtissues were functional by looking at their physiological response to contraction stimulations, using a muscle organ bath system (49) based on electrical pacing. To evaluate muscle force, MYOtissues were weighted and then transferred to the muscle strip chamber (**Figure 2G**). Before performing force analysis, both optimal length (Lo) and optimal frequency relationship were established to identify the optimal MYOtissues stretching and electric pulse frequency at which they developed peak of force (**Figure 2H**). The establishment of these parameters is essential to perform reliably muscle force comparisons between different types of MYOtissues. Indeed, Lo of fibroblast containing-MYOtissues was smaller than MYOtissues without fibroblasts as a result of more compact and stiff structure. We also verified that two weeks of maturation of the 3D culture was the optimal condition for functional evaluation. Indeed, at 3 weeks of culture, we detected a loss of contraction force. Isometric force analysis revealed significantly higher tetanic force in MYOtissue containing fibroblasts compared to the control, as (**Figure 2I**). Values were then normalized indirectly for the cross sectional area (CSA) using the

weight and Lo established for each MYOtissues for each MYOtissues (43,50) and expressed as specific tetanic force (mN/mm^2) (**Figure 2J**). In particular, the highest force with peak values ranging from 0.3 to 0.5 mN versus 0.1 to 0.2 mN in MYOtissues without fibroblasts after normalization (**Figure 2J**). These data demonstrated that MYOtissues plus fibroblasts have an improved structural organization and functional maturation that enables force contraction studies by electrical pacing.

DMD iPSC-derived MYOtissues display exacerbated pathogenic hallmarks

The improved muscle organization and functional maturation showed by iPSC-derived MYOtissues including fibroblasts, prompted us to exploit fibroblast features in disease modeling for DMD, where their role in disease progression is well known (14,15). We incorporated DMD fibroblasts as means to recapitulate the pathogenic microenvironment arising from their profibrotic activity exerted by tissue remodeling and matrix deposition (15,51). By this means we ultimately sought to reproduce the fibrotic-induced stiffness that could negatively affect contractile force of DMD MYOtissues, as it was shown previously in DMD cardiomyocytes (52). For that purpose, we used two DMD iPSC with different *DMD* mutations, a deletion of exon 45 (dEx45) or of exons 8-9 (dEx8-9) (53) together with human DMD immortalized fibroblasts, to generated DMD MYOtissues As control, two iPSC lines derived from healthy patients (Ctr1, Ctr2) were used and one representative (Ctr1) was carried for the further analysis after verifying comparable muscle differentiation and muscle performance. We additionally used as isogenic control, the DMD dEx8-9 iPSC corrected to restore dystrophin expression (53) (hereafter called corrDMD dEx8-9). Ctr or DMD MYOtissues were generated together with human healthy or DMD immortalized fibroblasts for histological, molecular and functional analyses. (**Figure 3A**). The myogenic differentiation of both Ctr and DMD iPSC lines was first tested in 2D and showed comparable differentiation efficiency. Histological characterization in MYOtissues, showed absence of Dystrophin protein in DMD MYOtissues and efficient myogenic differentiation and maturation in Ctr and DMD MYOtissues, as shown by the striated pattern visualized by SAA-stained sections (**Figure 3B**). We then monitored fibrotic hallmarks at histological level by looking at Fibronectin (Fn1), one of the major TGFβ target ECM gene and phosphorylated SMAD3 (pSMAD3), the transcriptional effector of canonical TGFβ pathway. Notably, DMD MYOtissues including DMD fibroblasts showed increase expression of Fn1 and increased number of pSMAD3 positive nuclei, indicating activation of TGFβ in DMD MYOtissues and fibrosis (**Figure 3B-C**). Presence of fibrosis within the DMD MYOtissues was also confirmed by the increased mRNA expression of Fn1 and Collagen 1

(Col1A) (**Figure 3D**). Additionally, we monitored the collagen secreted in the medium to further confirm the presence of fibrotic environment of DMD MYOtissues. For this aim, we used Collagen IV detecting assay, so to exclude the possibility to detect any contaminant Collagen coming from the matrix which is of type I. Notably, we observed an increase in Collagen IV released in the media of DMD MYOtissues, as compared to Ctr MYOtissues, that was significantly higher in the condition including fibroblasts (**Figure 3E**).

To assess whether DMD MYOtissues display hallmarks of DMD pathophysiology, we evaluated muscle function, that represents one of the most difficult challenges in the establishment of therapeutic readouts with *in vitro* systems. To identify reliable force parameters reflecting the defective DMD muscle performance, we subjected MYOtissues to isometric contractions (ISO) to measure tetanic force (**Figure 3F**), and to eccentric contractions (ECC) to assess muscle resistance and fatiguability (**Figure 3G**). As eccentric contraction plays a critical role in the disease progression of DMD (54) and repeated contractions trigger the degeneration/regeneration cycles (7), we used a specific ECC repetition protocol to assess muscle force loss and resistance under exhaustion. The protocol consisted of ten repetitions of ECC, where the force developed after each lengthening was calculated to trace muscle force drop over time. The drop force in both DMD dEx45 and dEx8-9-derived-MYOtissues (over 10 repetitions), was significantly higher than in control MYOtissues (Ctr1) and the corrected isogenic cell line (corrDMDdEx8-9) including or not fibroblasts (**Figure 3G**). To accurately quantify muscle fatigue, we calculated the fatigue index as drop of force between the isometric contractions performed before and after the 10x repetitions of ECC. The analysis showed a significant higher fatigue index in DMD MYOtissues as compared to Ctr MYOtissues and remarkably, this phenomenon was accentuated by the presence of fibroblasts. (**Figure 3H)**. Collectively these data indicate that DMD MYOtissues including dystrophic fibroblasts, displayed significant and exacerbated reduction of muscle resistance and increase of fatigue index (**Figure 3G-H)**, thereby defining them as the most appropriate system for further screenings. These data show that ECC-based drop force evaluation is a meaningful and reliable test to be used as therapeutic readouts as significant difference were detected between Ctr and DMD MYOtissues. These findings also indicate the necessity to activate and reveal the disease by mechanical challenges, which accelerates muscle fatigue in DMD MYOtissue as compared to Ctr MYOtissues.

AAV-µDystrophin gene transfer improves muscle resistance and restoration of DGC components

As proof of concept that MYOtissues were suitable as a screening platform for gene therapy products, we used AAV-mediated delivery of µDystrophin and assessed its therapeutic efficacy in the DMD context. For this aim, we used AAV9, as this serotype was used in recent clinical trials and showed high transduction rate in patients' myofibers (55,56). AAV9 infectivity in 3D engineered muscles was evaluated by a GFP reporter system (57), however in vitro µdystrophin AAV gene transfer, to the best of our knowledge, has not yet been reported. We first optimized the infection conditions using the reporter AAV9-CMV-GFP in Ctr MYOtissues including fibroblasts. Infections was performed at day 7 of the differentiation protocol, diluting AAV particles directly in the medium, and maintained for additional 7 days. We then used a codon optimized µDystrophin gene (dR4-23) under the control of the muscle specific sp512 promoter (19) for gene transfer using AAV9 (AAV9-µDys) in DMDdEx45 MYOtissues (**Figure 4A**). Low and high doses were established based on previous dosing studies to have intermediate transduction level at low dose (1E+9vg/MYOtissue), and high transduction level at high dose (5E+10vg/MYOtissue). Gene transfer efficiency was evaluated by quantification of Viral copy number (VCN) on genomic DNA extracted from MYOtissue and by expression level of the transgene and the encoded protein (**Figure 4B-D**). A clear dose-dependent entry of µDys increase of DNA, mRNA and protein levels were detected following AAV9-µDys gene transfer in the MYOtissues. Histological quantification of µDystrophin showed 30% of dystrophin positive myotubes at low dose compared to 95% in the high dose condition (**Figure 4E,** top panel).

Because dystrophin exerts its biomechanical support by holding the DGC in place, we monitored key components of the DGC, the transmembrane β-dystroglycan and the extra-cellular α-dystroglycan, whose proper expression and localization is impaired in the absence of Dystrophin (58). Immunostaining on transversal MYOtissues showed a dose-dependent yet not complete restoration of α- and β-dystroglycan (**Figure 4E,** middle and low panel). Interestingly, even high doses ensuring nearly total Dystrophin transduction did not fully restore α and β-dystroglycan, suggesting a potential therapeutic limitation of µDys. Overall, these data demonstrate the efficiency of µDystrophin gene transfer in DMD MYOtissues and partial, restoration of Dystrophin-associated components to the sarcolemma.

µDystrophin gene transfer rescues muscle strength and reduces the inflammatory milieu

To verify whether DGC restoration was associated to higher membrane stability and with protection from mechanical stress, Ctr and DMD MYOtissues treated or not with µDys were subjected to muscle force analysis (**Figure 5A**). Interestingly, isometric tetanic force analysis did not reveal any significant increase in DMDdEx45 MYOtissues following µDys delivery compared to not infected condition (**Figure 5B**). We then challenged the muscles by eccentric repetitions, and, under this condition, we observed a dose-dependent increase of muscle strength that reached significance only with high dose µDys (**Figure 5C**). Consistently with the acquired muscle resistance, the fatigue index was greatly reduced in DMD MYOtissues treated with high dose of µDys, close to the levels of Ctr MYOtissues (**Figure 5D**). These results were confirmed in MYOtissues derived from DMDdEx8-9 and its corrected isogenic control, where force analysis revealed improved muscle resistance and fatigue tolerance upon optimal µDys delivery. These data indicate that high dose µDys greatly improve muscle resistance and fatigue tolerance, whereas suboptimal transduction is not sufficient to significantly improve muscle strength, as shown by the partial gain of muscle strength in DMD dEx45-derived MYOtissues. One of the pathogenic hallmarks in damaged dystrophic muscle is the inflammatory response, mediated by proinflammatory cytokine release by myofibers, fibroblasts and infiltrating immune cells. For this aim, we looked at the secretion of Interleukin 1 (IL-1), Interleukin 6 (IL-6) and Tumor Necrosis Factor alpha (TNFα), (11,59) in DMD dEx45-derived MYOtissues. Conditioned media was collected 24h before and after the eccentric contraction repetitions to measure secretion of the proteins of interest. Remarkably, secretion of the three factors decreased significantly upon µDys restoration, in a dose-dependent manner and this effect was more important in the condition media after eccentric contractions (**Figure 5E**). These data confirmed the beneficial effect of µDys in improving the pathogenic milieu, likely as a result of improved membrane stability and reduced mechanical stress.

Discussion

The investigation and identification of new therapeutic strategies to face DMD is hampered by the lack of disease models that mimic adequately human pathology and could serve as a reliable screening platform. Here, we report the generation of 3D engineered muscles called MYOtissues, composed by a homogeneous population of myogenic cells derived from direct conversion of iPSC (13,40) combined with a population of fibroblasts, casted in a collagen-based matrix. We employed fibroblasts to reach a mature muscle structure that resulted in higher functional performance under muscle force evaluation. We then included human DMD fibroblasts to increase the severity of DMD iPSC derived-MYOtissues phenotype, driven by their profibrotic activity, as shown by exacerbated muscle force loss upon mechanical stress. By employing AAV-mediated µDys gene transfer, we demonstrated that DMD-MYOtissues highly transduced, recovered muscle resistance to eccentric contractions and partial membrane stability, with consequent amelioration of the inflammatory milieu. This evidence provides for the first time, the proof of principle of the suitability of DMD-MYOtissues as a reliable screening platform based on muscle strength assessment.

Reliable muscle function evaluation in engineered skeletal muscle tissues

Although several remarkable studies reported on muscle force in 3D models (39,53,60–62), muscle function evaluation is still a hurdle when coping with the difficulty in identifying disease-specific muscle force parameters, with the lack of an easy method to normalize muscle force and with the high variability of organoid models. Here we established parameters to evaluate muscle strength and fatigue index, defined as resistance to repeated eccentric contractions. These metrics, in addition to the already well-known correlation with the dystrophic phenotype (63), enables reliable force measurement independent of normalization, as it represents the ratio within the same engineered muscle tissue. Furthermore, our system showed reduce variability by minimizing intrinsic variabilities that could be caused by early defects during the pathogenesis. Several studies reported on a reduced myogenic differentiation ability in DMD-derived muscles, as compared to control. The difference in the myogenic gene expression pattern is likely due to the differentiation protocol used. As such, in protocol using chemical myogenic cocktails reproducing developmental cues it is more appropriate to detect early changes in DMD myopathies, while with direct transgene-based differentiation methods we can bypass and defective steps. As a result, our system aims at developing muscle artificial tissues from healthy or DMD iPSC that can be further challenged to activate and then reveal their pathogenic potential. This system has the advantage to be unbiased because we can perform muscle force analysis without considering the intrinsic contractile or myogenic defects that

would affecting muscle force necessarily (39,64,65). Therefore, we can perform screening in a reliable way, limiting intrinsic variables.

Activating DMD phenotype

Muscle development and differentiation requires cues elicited from the mesenchymal compartments (39,45). Since we used a transgene-based direct differentiation that bypasses the mesodermal/mesenchymal transition, we decided to use fibroblasts as they are the major component of the endomysium, the connective tissue surrounding the myofibers important for myofiber maturation (45,48). Fibroblasts were also shown to be important for self-assembly of the myofibers (42,47). We showed that including fibroblasts during the casting process, improved muscle alignment and the muscle force developed after electrical-induced contractions. Fibroblasts were mostly found in the external compartment of the 3D structure, surrounding and guiding muscle cells towards the same direction during differentiation, as shown by organized, elongated, and compact shape adopted when fibroblasts were included). As a result of the ameliorated muscle architecture and structural support, likely elicited by ECM production, fibroblasts containing-MYOtissues displayed more functional maturation and generated higher tetanus force during contraction.

We exploited fibroblasts also to exacerbate DMD phenotype until able to appreciate significant difference of the hallmarks of DMD pathology such as muscle function loss and fibrosis, caused by displacement of the DGC. For this purpose, we used DMD fibroblasts as a source of fibrotic cues to reproduce the pathogenic microenvironment and therefore exacerbate disease progression. Furthermore, is still unclear whether and how fibrosis impacts on contractility and muscle force in skeletal muscles. Recent studies shed light on the role of fibrosis-induced stiffness in contractile dysfunction of cardiomyocytes (52). It is tempting to hypothesize that pathogenic stiffening of muscle tissue is also involved in contraction defects and muscle force generation.

Collectively, our results showed that the use of severe modelling, characterize by a surrounding cytokine and fibrotic-rich milieu, and the use of a muscle exhaustion/fatigue test, allows improved modeling of DMD phenotype and enable reliable detection of pathological outcome once the muscle is stressed environmentally and mechanically.

Challenges and perspectives

By employing AAV-mediated delivery of µDys, the gold-standard in the DMD gene therapy, we proved that pro-fibrotic DMD MYOtissues efficiently transduced with µDys, recovered muscle strength and membrane stability. Interestingly, even high doses ensuring nearly total Dystrophin

transduction did not fully restore proper localization of key DGC members, opening the way to deeper interrogation of µDys efficacy. One limitation of our approach relates to the use of non-isogenic fibroblast cell lines to generate MYOtissues that can introduce variabilities due to different genetic backgrounds. However, this study aimed firstly at identifying the involvement of fibroblasts derived from a specific pathophysiological context in the exacerbation of the DMD pathogenic hallmarks for screening purposes. Indeed, as shown in different DMD iPSC lines, DMD fibroblasts inclusion, by its excessive matrix deposition, allows more faithful recapitulation of the fibrotic and inflammatory milieu that impact on muscle function and membrane stability. Overall, the exacerbated severity of DMD MYOtissues allows a broader window to evaluate therapeutic potential of AAV gene therapy products. Next-generation MYOtissues will then have to be derived using isogenic myogenic and fibroblast populations. Additionally, it would be of interest to recapitulate in our system, the role of fibroblasts and fibro-adipogenic progenitors in the disease progression and how their plasticity, activation and frequency is affected within a DMD muscle context, as shown recently in *in vivo* single-cell studies (66). Therefore, the inclusion of healthy fibroblasts in the generation of DMD MYOtissues can provide insights into their fibrogenic activation that contributes to the severity of the dystrophic phenotype.

By exacerbating the disease with DMD fibroblasts-dependent release of fibrotic cues and inflammatory cues. Notably, µDys delivery in DMD MYOtissues significantly attenuates the release of pro-inflammatory cytokines elicited by mechanical stress making our system suitable to integrate muscle function with the microenvironment. Thus, the MYOtissue platform provides the unique opportunity to associate the effect of gene transfer not only on the muscle function but also on the extracellular context that plays a key role in the initiation and progression of the disease. It will be interesting in the future to investigate the cross talk between muscle cells and fibroblasts that ultimately generate a pathogenic milieu in DMD muscles, that ultimately drives unbalanced immune response. In this regard, other cell populations such as macrophages, could be added in the MYOtissue to answer this question.

Because our protocol for muscle MYOtissue generation is fast, robust and allows large-scale testing, our system could be easily used as a testing platform not only for gene therapy but also to test pharmacological approaches. Thus, exacerbated MYOtissues provide a valuable human *in vitro* counterpart to animal *in vivo* preclinical studies, for a more stringent and reliable screening with the potential to accelerate the identifications of new treatments as wells as to unravel therapeutic limitations of current DMD treatments.

Materials and Methods

Experimental design

The objective of this study was to generate a human model of disease suitable for therapeutic screening or testing. We used control (Ctr) and DMD patients' iPSC to derive 3D muscle constructs, based on an optimized differentiation protocol and casting procedure, called MYOtissues. DMD MYOtissues were firstly characterized for their ability to recapitulate pathogenic features by histological evaluation in sections, gene expression analysis, secretome and force analysis. Of note, functional readouts were established in order to detect significant differences between Ctr and DMD MYOtissues such as eccentric contractions drop force analysis and fatigue index measurements. We then used DMD MYOtissue containing DMD fibroblasts to test the efficacy of gene therapy treatment using delivery of AAV9-µDys, by looking at the therapeutic readouts previously identified. Muscle force analysis after electrical-induced contractions, was performed looking at the tetanic force or at the drop force after eccentric contractions. At least 10 replicates (n, as indicated fin the figure legend) were used for each condition. Molecular and serum biomarker analysis was performed in the same MYOtissue right after the force measurements, while histological analysis was performed on other replicates not receiving electrical stimuli. For muscle force analysis, normalization for CSA was performed to reduce inter and intra-variability.

Cell culture and differentiation protocol

Human iPSCs used in the study were as follow: Ctr1 (AG08C5) derived from healthy fibroblasts (AG08498, Coriell Institute), Ctr2 (I-Stem), IPSC DMDdEx45 (Coriell, GM25313); DMDdEx8-9 and DMDdEx6-9 (corrected, isogenic control) (provided by Doctor E. Olson). iPSCs were maintained using mTeSRplus medium and passaged using ReleSR (Stem Cell Tech) on matrigel coated wells (Corning). iPSC engineering and muscle differentiation was performed adapting a transgene-based method previously described (13,40). Briefly, iPSC expressing inducible Baf60C and MyoD (iPSC^{BM}) were induced to express the transgenes by Doxycycline treatment in mTESRplus media. Then, iPSC^{BM} were dissociated and, either plated at 60k cells/cm², or resuspend in the hydrogel for 3D casting. For two-dimensional differentiation, the committed cells are kept in growth media (SKM02, AMSbiokit) supplemented with Doxycycline 200ng/ml for 2 days and then switched to differentiation media (SKM03 plus, AMSbiokit) supplemented with Doxycyclin 200 ng/ml for additional 5 days. Human immortalized fibroblasts from control (AB1191) and DMD patient (AB1024) were generated and obtained from Myobank-AFM of Myology Institute**.** Ctr and

DMD human immortalized fibroblasts, used in co-culture with hiPSC in 3D MYOtissues, were maintained in culture in 20% FBS DMEM Glutamax supplemented medium.

Generation of MYOtissues

MYOtissues from iPSC were generated adapting the protocol described for engineered heart tissue (67).Specifically,, 1.25 x 10^6 iPSC-committed (24 hours after induction with Doxycycline) are resuspended in 77 µl of growth media supplemented with hES cell Recovery (Stemgent) and molded in hydrogel composed by 40 µl of Bovine Collagen solution 6mg/ml (Sigma-Aldrich), 17.8 µl of Matrigel Growth Factor reduced (Corning) 10% v/v 3), 40µl 2X DMEM (Gibco) 4) and 5.2 µl of NaOH 1.5N 5). For the generation of MYOtissues including Fibroblasts, 1.25 x 10^5 (1:10) immortalized fibroblasts are included in the iPSC-committed mix during hydrogel preparation. The hydrogels are casted into 48-well plate TM5 MyrPlate (Myriamed), containing in each well a pair of flexible poles (static stretchers) that supports the growth of the engineered tissue in a ring shape. After 1 hour of polymerization at 37°C, media is added for 24 hours. At day 2 of the 3D, growth media (SKM02, AMSbiokit) is replaced by differentiation media (SKM03plus, AMSbiokit) and changed every day until day14.

Muscle force analysis

Functional analyses were carried out at day 14 after 3D casting. Contraction experiments were performed using the MyoDynamics Muscle Strip System 840 MD (DMT Technologies) and CS4 stimulator (DMT Technologies). All functional analysis were performed at 37°C, 5% CO_2 95% O2, in Tyrode's solution supplemented with 25 mM NaHCO3. Optimal muscle length was determined by gradually stretching the muscle until there was no further increase in the twitch tension. Functional tests were performed under isometric and eccentric conditions. MYOtissues were electrically stimulated with 250 pulses of 30V, 4ms width at the 125Hz of frequency for both isometric and eccentric contractions. For eccentric analysis, organoids were 1 mm stretched at the 6.5 cm/s during the muscular contraction. Each artificial tissue was subjected to 1 isometric contraction, 10 eccentric contractions and 1 isometric contraction. Data collection and analysis was done by PowerLab device and LabChart software (AD instruments) respectively. Fatigue is represented as percentage drop force between the first and the last isometric contraction. Where indicated, force is indirectly normalized for the CSA (Cross Section Area) calculated as muscle force (mN) x Lo (mm) x density (mg/mm^3)/weight (mg) and expressed as mN/mm^2. Muscle density is experimentally determined as 2.089 mg/mm^3.

Electron Microscopy studies

Electron microscopy analysis was prospectively performed on MYOtissue specimens that were fixed with glutaraldehyde (2.5%, pH 7.4), post fixed with osmium tetroxide (2%), dehydrated in a graded series of ethanol ranging from 30% to absolute solution and embedded in resin (EMBed-812, Electron Microscopy Sciences, USA). Ultra-thin sections from at least four blocks from WT iPSC-derived Organoids in presence or absence of WT fibroblasts were stained with uranyl acetate and lead citrate. The grids were observed using a "JEOL 1400 Flash" electron microscope (120 kV) and were photo documented using a Xarosa camera (Soft Imaging System, France).

Immunofluorescence

MYOtissues are fixed if 4% methanol-free PFA overnight at day 14. For whole mount staining, fixed MYOtissues were permeabilized, stained and dehydrated with the MACS clearing kit (Miltenyi) accordingly to manufacturer's instructions. Whole mount-stained organoids are then imaged with confocal microscope (LEICA STED SP8) at 10X magnification.

For staining on transversal or longitudinal sections, fixed MYOtissues are dehydrated with a gradient of sucrose (7.5%-30%) over-day and embedded in OCT matrix in plastic mold. After 24 hr, embedded organoids are processed with the cryostat (LEICA) with 15 µm thick sections. Slices were then dried and fixed again with 4% methanol-free PFA (Invitrogen). Fixed sections are then blocked with serum cocktail (5% Goat serum and 5% Fetal bovine serum), before being stained overnight at +4°C with primary antibody. After that, slices are washed three times in PBS and hybridized with AlexaFluor secondary antibody accordingly to the host species of the first antibody. Stained slides were then covered with Fluoromont + Dapi and glass slide 1.5H. For imaging, sections are scanned with AxioScan microscope and confocal Leica SP8. FIJI and CellPose was used for images analysis. Myotube alignment was determined by angles measurement function (FIJI). Myotubes circularity was determined by custom FIJI script. Briefly, myotubes cross section area was first segmented by pre-trained Cellpose2 *cyto2* model (68) and then converted into Regions of Interest (ROIs) by *Labels_To_Rois.py* plugin (69) for subsequent quantification on FIJI (Ferret diameters X and Y).

Gene expression analysis

For gene expression analysis, RNA was isolated from MYOtissues by RNeasy micro kit (QIAGEN) accordingly to manufacturer's instructions, controlled and quantify by Nanodrop. 0.5-1µg of RNA was retro-transcribed to cDNA thanks to the RevertAid H Minus First Strand cDNA

Synthesis Kit (Invitrogen). Droplet digital PCR was performed to assess the expression of myogenic factors (MyoD, Myh2, Myh7, MCK), of fibrotic markers (Col1A, Fn1) and µDystrophin, thanks to the QX200™ ddPCR™ EvaGreen Supermix (Biorad). Gene expression results in copy/µl are represented as fold change to the expression of MyoD normalized for GAPDH housekeeping gene.

Biomarker analysis from conditioned media

Secretome analysis was performed using the MILLIPLEX® Multiplex Assays Using Luminex® Technology (Millipore), accordingly to manufacturer's instructions.

AAV production and organoids infection

Recombinant AAV were produced as previously described (70) using AAV9 serotype. Purification was performed using affinity chromatography and titration was done by ddPCR using ITRs primers. For optimization of infection, an AAV9-CMV-GFP construct was used. The micro-dystrophin transgene used in the study, under the control of spc512 promoter, was an optimized version of construct used for GENETHON's preclinical investigation and clinical trial (71), with deletion from spectrin-like repeats 4 to 23 and full C-terminal truncation, here referred as µDys. Infection in organoids was performed delivering the AAV9 particles diluted into the differentiation media at day 7, at two different doses: 1E+10 vg/organoids (low dose) and 5E+10 vg/organoids (high dose). Media was replaced after 24 hr from the infection and changed daily until day 14.

Viral copy number analysis

Viral DNA was extracted from mature MYOtissues by NucleoMag Pathogen kit (Macherey Nagel) using Kingfisher instrument (Thermofisher). DNA yield and purity was assessed by Nanodrop; VCN (viral copy number) was identified by droplet digital PCR using supermix for probe (Biorad). Results are shown as copy number variation using P0 as reference DNA.

Capillary western blot analysis

MYOtissues proteins were extracted in RIPA buffer supplemented with Protease Inhibitor Cocktail EDTA-free (Roche) and Benzonase by homogenization. Total proteins were then quantified by BCA method, thanks to the Pierce BCA protein assay kit (Invitrogen) accordingly to manufacturer's instructions. Protein detection has been performed by capillary western blot, thanks to the JESS protein simple (Bio-techne), accordingly to manufacturer's directions. Micro-

dystrophin detection has been performed by the antibody DysB (NCL-DYSB, Leica, 1:20) and its expression has been quantified by total protein normalization.

Statistical analysis

All data were analyzed by GraphPad Prism 9.5.1 software. Error bars on plots represent the standard error of the mean (SEM). Statistical significance was determined by either one-way or two-way analysis of variance (ANOVA) with Tukey's correction for multiple comparison tests. Results were considered significant at $p < 0.05$.

Acknowledgments

We express our gratitude to Rene Hummel (DMT), Guillaume Tanniou, and Nicolas Guerchet for their invaluable technical support in muscle force evaluation. We also extend our appreciation to Jérémie for the assistance in imaging and to the histology team for their technical expertise. Finally, we would like to thank Frederique Magdinier for generously providing the DMD iPSC dEx45 and Ctr1 iPSC.

Funding: This study was financially supported by the Institut National de la Sante et de la Recherche Medicale (INSERM)

Author contributions:

SA and LP designed the experiments. LP performed the majority of the experiments, including iPSC culture, organoid generation, imaging and muscle force analysis. AJ analyzed conditioned media biomarkers and performed secretome analysis. MM contributed to muscle force analysis. RE and GB performed electron microscopy analysis. AB generated and provided the immortalized human fibroblasts. SA and LP performed data analysis and figures preparation. SA conceived, supervised the project, and wrote the manuscript. All authors discussed results. SA, LP, DI and IR reviewed and edited the manuscript reviewed, and edited the manuscript.

Competing interests: All other authors declare they have no competing interests.

Data and materials availability: (MTAs). All data are available in the main text or the supplementary materials. The DMD-iPSC dEx8-9 and isogenic corrected control (iPSC dEx6-9) were provided by Dr Eric Olson while the Ctr2 iPSC line by I-Stem, upon MTA.

References

1. Mendell JR, Shilling C, Leslie ND, Flanigan KM, Al-Dahhak R, Gastier-Foster J, et al. Evidence-based path to newborn screening for Duchenne muscular dystrophy. Ann Neurol [Internet]. 2012 Mar [cited 2022 Oct 13];71(3):304–13. Available from: https://pubmed.ncbi.nlm.nih.gov/22451200/
2. Ervasti JM, Campbell KP. A role for the dystrophin-glycoprotein complex as a transmembrane linker between laminin and actin. J Cell Biol [Internet]. 1993 [cited 2023 Apr 18];122(4):809–23. Available from: https://pubmed.ncbi.nlm.nih.gov/8349731/
3. Petrof BJ, Shrager JB, Stedman HH, Kelly AM, Sweeney HL. Dystrophin protects the sarcolemma from stresses developed during muscle contraction. Proc Natl Acad Sci U S A [Internet]. 1993 Apr 15 [cited 2023 Apr 18];90(8):3710–4. Available from: https://pubmed.ncbi.nlm.nih.gov/8475120/
4. Hoffman EP, Brown RH, Kunkel LM. Dystrophin: the protein product of the Duchenne muscular dystrophy locus. Cell [Internet]. 1987 Dec 24 [cited 2022 Oct 13];51(6):919–28. Available from: https://pubmed.ncbi.nlm.nih.gov/3319190/
5. Hoffman EP. The discovery of dystrophin, the protein product of the Duchenne muscular dystrophy gene. FEBS J [Internet]. 2020 Sep 1 [cited 2021 Mar 5];287(18):3879–87. Available from: https://pubmed.ncbi.nlm.nih.gov/32608079/
6. Hoffman EP, Brown RH, Kunkel LM. Dystrophin: the protein product of the Duchenne muscular dystrophy locus. Cell [Internet]. 1987 Dec 24 [cited 2023 Apr 18];51(6):919–28. Available from: https://pubmed.ncbi.nlm.nih.gov/3319190/
7. Elangkovan N, Dickson G. Gene Therapy for Duchenne Muscular Dystrophy. J Neuromuscul Dis [Internet]. 2021 [cited 2023 Apr 20];8(Suppl 2):S303. Available from: /pmc/articles/PMC8673537/
8. Gao QQ, McNally EM. The dystrophin complex: Structure, function, and implications for therapy. Compr Physiol [Internet]. 2015 Jul 1 [cited 2021 Mar 5];5(3):1223–39. Available from: https://pubmed.ncbi.nlm.nih.gov/26140716/
9. Davies KE, Nowak KJ. Molecular mechanisms of muscular dystrophies: old and new players. Nat Rev Mol Cell Biol [Internet]. 2006 Oct 23 [cited 2023 Apr 20];7(10):762–73. Available from: https://pubmed.ncbi.nlm.nih.gov/16971897/
10. Ennen JP, Verma M, Asakura A. Vascular-targeted therapies for Duchenne muscular dystrophy. Skelet Muscle [Internet]. 2013 Apr 23 [cited 2023 Apr 20];3(1). Available from: https://pubmed.ncbi.nlm.nih.gov/23618411/

11. Porter JD, Khanna S, Kaminski HJ, Sunil Rao J, Merriam AP, Richmonds CR, et al. A chronic inflammatory response dominates the skeletal muscle molecular signature in dystrophin-deficient mdx mice. Hum Mol Genet [Internet]. 2002 Feb 1 [cited 2023 Jun 27];11(3):263–72. Available from: https://pubmed.ncbi.nlm.nih.gov/11823445/
12. Amor F, Vu Hong A, Corre G, Sanson M, Suel L, Blaie S, et al. Cholesterol metabolism is a potential therapeutic target in Duchenne muscular dystrophy. J Cachexia Sarcopenia Muscle [Internet]. 2021 Jun 1 [cited 2023 Jul 5];12(3):677–93. Available from: https://pubmed.ncbi.nlm.nih.gov/34037326/
13. Caputo L, Granados A, Lenzi J, Rosa A, Ait-Si-Ali S, Puri PL, et al. Acute conversion of patient-derived Duchenne muscular dystrophy iPSC into myotubes reveals constitutive and inducible over-activation of TGFβ-dependent pro-fibrotic signaling. Skelet Muscle. 2020 May 2;10(1).
14. Wynn TA. Cellular and molecular mechanisms of fibrosis. J Pathol. 2008 Jan;214(2):199–210.
15. Kharraz Y, Guerra J, Pessina P, Serrano AL, Muñoz-Cánoves P. Understanding the process of fibrosis in Duchenne muscular dystrophy. Biomed Res Int [Internet]. 2014 [cited 2018 Sep 7];2014:965631. Available from: http://www.hindawi.com/journals/bmri/2014/965631/
16. Mendell JR, Al-Zaidy SA, Rodino-Klapac LR, Goodspeed K, Gray SJ, Kay CN, et al. duan. Mol Ther [Internet]. 2021 Feb 3 [cited 2023 Apr 18];29(2):464–88. Available from: https://pubmed.ncbi.nlm.nih.gov/33309881/
17. Aguti S, Malerba A, Zhou H. The progress of AAV-mediated gene therapy in neuromuscular disorders. Expert Opin Biol Ther [Internet]. 2018 Jun 3 [cited 2023 Apr 18];18(6):681–93. Available from: https://pubmed.ncbi.nlm.nih.gov/29781327/
18. Duan D. Systemic AAV Micro-dystrophin Gene Therapy for Duchenne Muscular Dystrophy. Mol Ther [Internet]. 2018 Oct 3 [cited 2023 Apr 18];26(10):2337–56. Available from: https://linkinghub.elsevier.com/retrieve/pii/S1525001618303368
19. Le Guiner C, Servais L, Montus M, Larcher T, Fraysse B, Moullec S, et al. Long-term microdystrophin gene therapy is effective in a canine model of Duchenne muscular dystrophy. Nat Commun [Internet]. 2017 Jul 25 [cited 2021 Mar 1];8. Available from: https://pubmed.ncbi.nlm.nih.gov/28742067/
20. Elangkovan N, Dickson G. Gene Therapy for Duchenne Muscular Dystrophy. J Neuromuscul Dis [Internet]. 2021 [cited 2023 Apr 20];8(s2):S303–16. Available from: https://pubmed.ncbi.nlm.nih.gov/34511510/

21. Harper SQ, Hauser MA, DelloRusso C, Duan D, Crawford RW, Phelps SF, et al. Modular flexibility of dystrophin: implications for gene therapy of Duchenne muscular dystrophy. Nat Med [Internet]. 2002 [cited 2023 Apr 20];8(3):253–61. Available from: https://pubmed.ncbi.nlm.nih.gov/11875496/

22. Wang B, Li J, Xiao X. Adeno-associated virus vector carrying human minidystrophin genes effectively ameliorates muscular dystrophy in mdx mouse model. Proc Natl Acad Sci U S A [Internet]. 2000 Dec 5 [cited 2023 Apr 20];97(25):13714–9. Available from: https://pubmed.ncbi.nlm.nih.gov/11095710/

23. Duan D. Duchenne Muscular Dystrophy Gene Therapy in 2023: Status, Perspective, and Beyond. Hum Gene Ther [Internet]. 2023 May 1 [cited 2023 Jul 6];34(9–10):345–9. Available from: https://pubmed.ncbi.nlm.nih.gov/37219994/

24. Birch SM, Lawlor MW, Conlon TJ, Guo LJ, Crudele JM, Hawkins EC, et al. Assessment of systemic AAV-microdystrophin gene therapy in the GRMD model of Duchenne muscular dystrophy. Sci Transl Med [Internet]. 2023 Jan 4 [cited 2023 Jun 14];15(677):eabo1815. Available from: https://pubmed.ncbi.nlm.nih.gov/36599002/

25. Bostick B, Shin JH, Yue Y, Wasala NB, Lai Y, Duan D. AAV micro-dystrophin gene therapy alleviates stress-induced cardiac death but not myocardial fibrosis in >21-m-old mdx mice, an end-stage model of Duchenne muscular dystrophy cardiomyopathy. J Mol Cell Cardiol [Internet]. 2012 Aug [cited 2023 Jun 14];53(2):217–22. Available from: https://pubmed.ncbi.nlm.nih.gov/22587991/

26. Takahashi K, Tanabe K, Ohnuki M, Narita M, Ichisaka T, Tomoda K, et al. Induction of Pluripotent Stem Cells from Adult Human Fibroblasts by Defined Factors. Cell [Internet]. 2007 Nov 30 [cited 2021 Mar 5];131(5):861–72. Available from: https://pubmed.ncbi.nlm.nih.gov/18035408/

27. Tornabene P, Trapani I, Minopoli R, Centrulo M, Lupo M, De Simone S, et al. Intein-mediated protein trans-splicing expands adeno-associated virus transfer capacity in the retina. Sci Transl Med [Internet]. 2019 [cited 2023 Mar 30];11(492). Available from: https://pubmed.ncbi.nlm.nih.gov/31092694/

28. Clevers H. Modeling Development and Disease with Organoids. Cell [Internet]. 2016 Jun 16 [cited 2023 Apr 18];165(7):1586–97. Available from: https://pubmed.ncbi.nlm.nih.gov/27315476/

29. Hofer M, Lutolf MP. Engineering organoids. Nat Rev Mater [Internet]. 2021 May 1 [cited 2023 Apr 18];6(5):402–20. Available from: https://pubmed.ncbi.nlm.nih.gov/33623712/

30. Kruczek K, Qu Z, Gentry J, Fadl BR, Gieser L, Hiriyanna S, et al. Gene Therapy of Dominant CRX-Leber Congenital Amaurosis using Patient Stem Cell-Derived Retinal Organoids. Stem cell reports [Internet]. 2021 Feb 9 [cited 2023 Apr 19];16(2):252–63. Available from: https://pubmed.ncbi.nlm.nih.gov/33513359/
31. Khabou H, Garita-Hernandez M, Chaffiol A, Reichman S, Jaillard C, Brazhnikova E, et al. Noninvasive gene delivery to foveal cones for vision restoration. JCI insight [Internet]. 2018 Jan 25 [cited 2023 Apr 19];3(2). Available from: https://pubmed.ncbi.nlm.nih.gov/29367457/
32. Garita-Hernandez M, Routet F, Guibbal L, Khabou H, Toualbi L, Riancho L, et al. AAV-Mediated Gene Delivery to 3D Retinal Organoids Derived from Human Induced Pluripotent Stem Cells. Int J Mol Sci [Internet]. 2020 Feb 1 [cited 2023 Mar 30];21(3). Available from: https://pubmed.ncbi.nlm.nih.gov/32028585/
33. Garita-Hernandez M, Routet F, Guibbal L, Khabou H, Toualbi L, Riancho L, et al. AAV-Mediated Gene Delivery to 3D Retinal Organoids Derived from Human Induced Pluripotent Stem Cells. Int J Mol Sci [Internet]. 2020 Feb 1 [cited 2023 Apr 19];21(3). Available from: https://pubmed.ncbi.nlm.nih.gov/32028585/
34. Ramamurthy RM, Atala A, Porada CD, Almeida-Porada G. Organoids and microphysiological systems: Promising models for accelerating AAV gene therapy studies. Front Immunol [Internet]. 2022 Sep 26 [cited 2023 Apr 19];13. Available from: https://pubmed.ncbi.nlm.nih.gov/36225917/
35. Chemello F, Chai AC, Li H, Rodriguez-Caycedo C, Sanchez-Ortiz E, Atmanli A, et al. Precise correction of Duchenne muscular dystrophy exon deletion mutations by base and prime editing. Sci Adv [Internet]. 2021 Apr 1 [cited 2023 Apr 20];7(18). Available from: https://pubmed.ncbi.nlm.nih.gov/33931459/
36. Shin MK, Bang JS, Lee JE, Tran HD, Park G, Lee DR, et al. Generation of Skeletal Muscle Organoids from Human Pluripotent Stem Cells to Model Myogenesis and Muscle Regeneration. Int J Mol Sci [Internet]. 2022 May 1 [cited 2023 Apr 20];23(9). Available from: /pmc/articles/PMC9103168/
37. Pinton L, Khedr M, Lionello VM, Sarcar S, Maffioletti SM, Dastidar S, et al. 3D human induced pluripotent stem cell-derived bioengineered skeletal muscles for tissue, disease and therapy modeling. Nat Protoc [Internet]. 2023 [cited 2023 Apr 18];18(4). Available from: https://pubmed.ncbi.nlm.nih.gov/36792780/
38. Rao L, Qian Y, Khodabukus A, Ribar T, Bursac N. Engineering human pluripotent stem cells into a functional skeletal muscle tissue. Nat Commun [Internet]. 2018 Dec 9

[cited 2018 Oct 16];9(1):126. Available from: http://www.nature.com/articles/s41467-017-02636-4

39. Shahriyari M, Islam MR, Sakib SM, Rinn M, Rika A, Krüger D, et al. Engineered skeletal muscle recapitulates human muscle development, regeneration and dystrophy. J Cachexia Sarcopenia Muscle. 2022 Dec 1;13(6):3106–21.

40. Albini S, Coutinho P, Malecova B, Giordani L, Savchenko A, Forcales SV, et al. Epigenetic Reprogramming of Human Embryonic Stem Cells into Skeletal Muscle Cells and Generation of Contractile Myospheres. Cell Rep. 2013;3(3):661–70.

41. Albini S, Puri PL. Generation of Myospheres From hESCs by Epigenetic Reprogramming. J Vis Exp [Internet]. 2014;(88). Available from: http://www.jove.com/video/51243/generation-of-myospheres-from-hescs-by-epigenetic-reprogramming

42. Li M, Dickinson CE, Finkelstein EB, Neville CM, Sundback CA. The role of fibroblasts in self-assembled skeletal muscle. Tissue Eng Part A [Internet]. 2011 Nov 1 [cited 2023 Apr 1];17(21–22):2641–50. Available from: https://pubmed.ncbi.nlm.nih.gov/21657983/

43. Santos GL, Meyer T, Tiburcy M, Degrave A, Zimmermann WH, Lutz S. Fibroblast Derived Human Engineered Connective Tissue for Screening Applications. J Vis Exp [Internet]. 2021 Aug 1 [cited 2023 Apr 18];2021(174). Available from: https://pubmed.ncbi.nlm.nih.gov/34487119/

44. Kühl U, Öcalan M, Timpl R, Mayne R, Hay E, von der Mark K. Role of muscle fibroblasts in the deposition of type-IV collagen in the basal lamina of myotubes. Differentiation [Internet]. 1984 [cited 2023 Apr 1];28(2):164–72. Available from: https://pubmed.ncbi.nlm.nih.gov/6396135/

45. Mathew SJ, Hansen JM, Merrell AJ, Murphy MM, Lawson JA, Hutcheson DA, et al. Connective tissue fibroblasts and Tcf4 regulate myogenesis. Development [Internet]. 2011 Jan 15 [cited 2023 Apr 7];138(2):371–84. Available from: https://pubmed.ncbi.nlm.nih.gov/21177349/

46. Tiburcy M, Meyer T, Soong PL, Zimmermann WH. Collagen-based engineered heart muscle. Methods Mol Biol [Internet]. 2014 [cited 2023 Apr 20];1181:167–76. Available from: https://pubmed.ncbi.nlm.nih.gov/25070336/

47. Rao N, Evans S, Stewart D, Spencer KH, Sheikh F, Hui EE, et al. Fibroblasts influence muscle progenitor differentiation and alignment in contact independent and dependent manners in organized co-culture devices. Biomed Microdevices [Internet]. 2013 Feb

[cited 2023 Apr 25];15(1):161. Available from: /pmc/articles/PMC3537877/

48. Bersini S, Gilardi M, Ugolini GS, Sansoni V, Talò G, Perego S, et al. Engineering an Environment for the Study of Fibrosis: A 3D Human Muscle Model with Endothelium Specificity and Endomysium. Cell Rep [Internet]. 2018 Dec 26 [cited 2023 Apr 24];25(13):3858-3868.e4. Available from: https://pubmed.ncbi.nlm.nih.gov/30590054/

49. Minato K, Yoshimoto Y, Kurosawa T, Watanabe K, Kawashima H, Ikemoto-Uezumi M, et al. Measurement of Lateral Transmission of Force in the Extensor Digitorum Longus Muscle of Young and Old Mice. Int J Mol Sci [Internet]. 2021 Nov 1 [cited 2023 Apr 28];22(22). Available from: /pmc/articles/PMC8623005/

50. Erdogan BR, Karaomerlioglu I, Yesilyurt ZE, Ozturk N, Muderrisoglu AE, Michel MC, et al. Normalization of organ bath contraction data for tissue specimen size: does one approach fit all? Naunyn Schmiedebergs Arch Pharmacol [Internet]. 2020 Feb 1 [cited 2023 Apr 28];393(2):243–51. Available from: https://pubmed.ncbi.nlm.nih.gov/31511953/

51. Mann CJ, Perdiguero E, Kharraz Y, Aguilar S, Pessina P, Serrano AL, et al. Aberrant repair and fibrosis development in skeletal muscle. Skelet Muscle [Internet]. 2011 May 4 [cited 2023 Apr 28];1(1):21. Available from: /pmc/articles/PMC3156644/

52. Chang ACY, Pardon G, Chang ACH, Wu H, Ong SG, Eguchi A, et al. Increased tissue stiffness triggers contractile dysfunction and telomere shortening in dystrophic cardiomyocytes. Stem cell reports [Internet]. 2021 Sep 14 [cited 2023 Apr 20];16(9):2169–81. Available from: https://pubmed.ncbi.nlm.nih.gov/34019816/

53. Kyrychenko V, Kyrychenko S, Tiburcy M, Shelton JM, Long C, Schneider JW, et al. Functional correction of dystrophin actin binding domain mutations by genome editing. JCI insight [Internet]. 2017 Sep 21 [cited 2023 Apr 3];2(18). Available from: https://pubmed.ncbi.nlm.nih.gov/28931764/

54. Childers MK, Okamura CS, Bogan DJ, Bogan JR, Petroski GF, McDonald K, et al. Eccentric contraction injury in dystrophic canine muscle. Arch Phys Med Rehabil [Internet]. 2002 Nov 1 [cited 2023 Apr 3];83(11):1572–8. Available from: https://pubmed.ncbi.nlm.nih.gov/12422328/

55. Manini A, Abati E, Nuredini A, Corti S, Comi G Pietro. Adeno-Associated Virus (AAV)-Mediated Gene Therapy for Duchenne Muscular Dystrophy: The Issue of Transgene Persistence. Front Neurol [Internet]. 2021 Jan 5 [cited 2023 Apr 25];12:814174. Available from: /pmc/articles/PMC8797140/

56. Aguti S, Malerba A, Zhou H. The progress of AAV-mediated gene therapy in

neuromuscular disorders. Expert Opin Biol Ther [Internet]. 2018 Jun 3 [cited 2023 Apr 25];18(6):681–93. Available from: https://pubmed.ncbi.nlm.nih.gov/29781327/

57. Pinton L, Khedr M, Lionello VM, Sarcar S, Maffioletti SM, Dastidar S, et al. 3D human induced pluripotent stem cell-derived bioengineered skeletal muscles for tissue, disease and therapy modeling. Nat Protoc [Internet]. 2023 [cited 2023 Apr 1]; Available from: https://pubmed.ncbi.nlm.nih.gov/36792780/

58. Lapidos KA, Kakkar R, McNally EM. The dystrophin glycoprotein complex: signaling strength and integrity for the sarcolemma. Circ Res [Internet]. 2004 Apr 30 [cited 2023 Jun 27];94(8):1023–31. Available from: https://pubmed.ncbi.nlm.nih.gov/15117830/

59. Rosenberg AS, Puig M, Nagaraju K, Hoffman EP, Villalta SA, Rao VA, et al. Immune-mediated pathology in Duchenne muscular dystrophy. Sci Transl Med [Internet]. 2015 Aug 5 [cited 2018 Sep 7];7(299):299rv4-299rv4. Available from: http://www.ncbi.nlm.nih.gov/pubmed/26246170

60. Madden L, Juhas M, Kraus WE, Truskey GA, Bursac N. Bioengineered human myobundles mimic clinical responses of skeletal muscle to drugs. Elife [Internet]. 2015 Jan 8 [cited 2023 Apr 13];4(4). Available from: https://pubmed.ncbi.nlm.nih.gov/25575180/

61. Rao L, Qian Y, Khodabukus A, Ribar T, Bursac N. Engineering human pluripotent stem cells into a functional skeletal muscle tissue. Nat Commun [Internet]. 2018 Dec 1 [cited 2023 Apr 13];9(1). Available from: https://pubmed.ncbi.nlm.nih.gov/29317646/

62. Khodabukus A, Madden L, Prabhu NK, Koves TR, Jackman CP, Muoio DM, et al. Electrical stimulation increases hypertrophy and metabolic flux in tissue-engineered human skeletal muscle. Biomaterials [Internet]. 2018 Aug 31 [cited 2018 Oct 29]; Available from: http://www.ncbi.nlm.nih.gov/pubmed/30180985

63. Barton ER, Lynch G, Khurana TS, Raymackers J-M, Dorchies O, Carlson G. Measuring isometric force of isolated mouse muscles in vitro. 2008;

64. Chal J, Oginuma M, Al Tanoury Z, Gobert B, Sumara O, Hick A, et al. Differentiation of pluripotent stem cells to muscle fiber to model Duchenne muscular dystrophy. Nat Biotechnol [Internet]. 2015 Sep 3 [cited 2018 Sep 7];33(9):962–9. Available from: http://www.nature.com/articles/nbt.3297

65. Al Tanoury Z, Zimmerman JF, Rao J, Sieiro D, McNamara HM, Cherrier T, et al. Prednisolone rescues Duchenne muscular dystrophy phenotypes in human pluripotent stem cell-derived skeletal muscle in vitro. Proc Natl Acad Sci U S A [Internet]. 2021 Jul 13 [cited 2023 Apr 24];118(28). Available from:

https://pubmed.ncbi.nlm.nih.gov/34260377/

66. Saleh KK, Xi H, Switzler C, Skuratovsky E, Romero MA, Chien P, et al. Single cell sequencing maps skeletal muscle cellular diversity as disease severity increases in dystrophic mouse models. iScience [Internet]. 2022 Nov 18 [cited 2023 Jul 9];25(11). Available from: http://www.cell.com/article/S258900422201687X/fulltext

67. Tiburcy M, Meyer T, Liaw NY, Zimmermann WH. Generation of Engineered Human Myocardium in a Multi-well Format. STAR Protoc [Internet]. 2020 Jun 19 [cited 2023 Apr 26];1(1). Available from: https://pubmed.ncbi.nlm.nih.gov/33111083/

68. Stringer C, Wang T, Michaelos M, Pachitariu M. Cellpose: a generalist algorithm for cellular segmentation. Nat Methods [Internet]. 2021 Jan 1 [cited 2023 Jun 28];18(1):100–6. Available from: https://pubmed.ncbi.nlm.nih.gov/33318659/

69. Waisman A, Norris AM, Elías Costa M, Kopinke D. Automatic and unbiased segmentation and quantification of myofibers in skeletal muscle. Sci Rep [Internet]. 2021 Dec 1 [cited 2023 Jun 28];11(1). Available from: https://pubmed.ncbi.nlm.nih.gov/34083673/

70. Bourg N, Hong AV, Lostal W, Jaber A, Guerchet N, Tanniou G, et al. Co-Administration of Simvastatin Does Not Potentiate the Benefit of Gene Therapy in the mdx Mouse Model for Duchenne Muscular Dystrophy. Int J Mol Sci [Internet]. 2022 Feb 1 [cited 2023 Jun 23];23(4). Available from: https://pubmed.ncbi.nlm.nih.gov/35216132/

71. Le Guiner C, Servais L, Montus M, Larcher T, Fraysse B, Moullec S, et al. Long-term microdystrophin gene therapy is effective in a canine model of Duchenne muscular dystrophy. Nat Commun [Internet]. 2017 Jul 25 [cited 2023 Mar 28];8. Available from: https://pubmed.ncbi.nlm.nih.gov/28742067/

Acknowledgments

We express our gratitude to Rene Hummel (DMT), Guillaume Tanniou, and Nicolas Guerchet for the invaluable technical support in muscle force evaluation. We also extend our appreciation to Jérémie for the assistance in imaging and to the histology team for their technical expertise. Finally, we would like to thank Frederique Magdinier for generously providing the DMD iPSC dEx45 and Ctr1 iPSC.

MAIN FIGURES

Figure 1

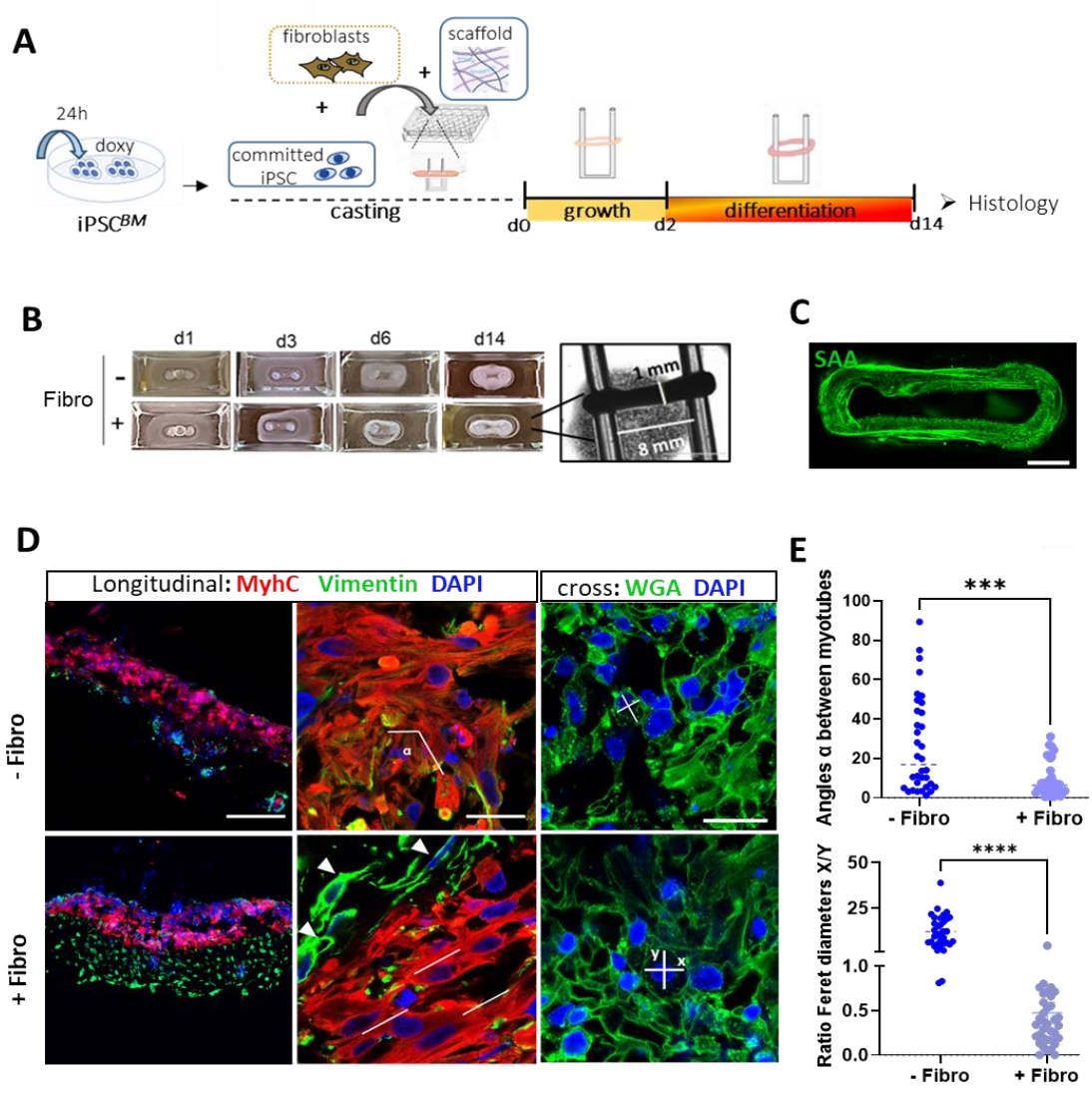

Figure 1. Generation of iPSC-derived MYOtissues and impact of fibroblasts inclusion on muscle organization. ***(A)*** *Scheme of the protocol used to generate muscle artificial tissues (MYOtissues) from iPSC committed towards the myogenic lineage by 24h treatment with doxycycline for inducible expression of MyoD and BAF60C transgenes (iPSC^{BM}). Casting procedure included: committed iPSC, fibroblasts when indicated (+/-fibro) and a collagen-based scaffold, within a 48 well plate equipped with silicon pillars. After 2 days in growth medium, the 3D structures were shifted in differentiation medium until day 14 for histological analysis.* ***(B)*** *Condensation kinetics of MYOtissues +/-fibro.* ***(C)*** *Whole-mount staining of MYOtissues with Sarcomeric α-Actinin (SAA) and 3D reconstruction of the ring-shaped constructs using confocal imaging. Scale bar: 1mm.* ***(D)*** *Representative longitudinal and cross sections of MYOtissues +/- fibroblasts, immunostained for Myosin Heavy Chain (MyHC) and Vimentin or for wheat germ agglutinin (WGA). Nuclei were visualized with DAPI. Scale bars 200µm (left panel) and 10 µm (middle and right panel). Arrows indicate fibroblasts recruited adjacently to the muscle fibers;*

α is the angle formed between myotubes; lines indicate aligned myotubes, crosses represent X/Y myotubes diameters. ***(E)*** *The alignment was calculated based on the angle (α) formed between myotubes (α close to 0 corresponds to aligned myotubes, while far from 0 corresponds to not aligned myotubes), while circularity from X/Y myotubes diameters ratio (ratio 1 circular, far from 1 not circular). Data were collected from 3 independent experiments with at least 3 replicates. Unpaired two-tailed t-test was used (**$p \leq 0.01$, ****$p \leq 0.0001$).*

Figure 2

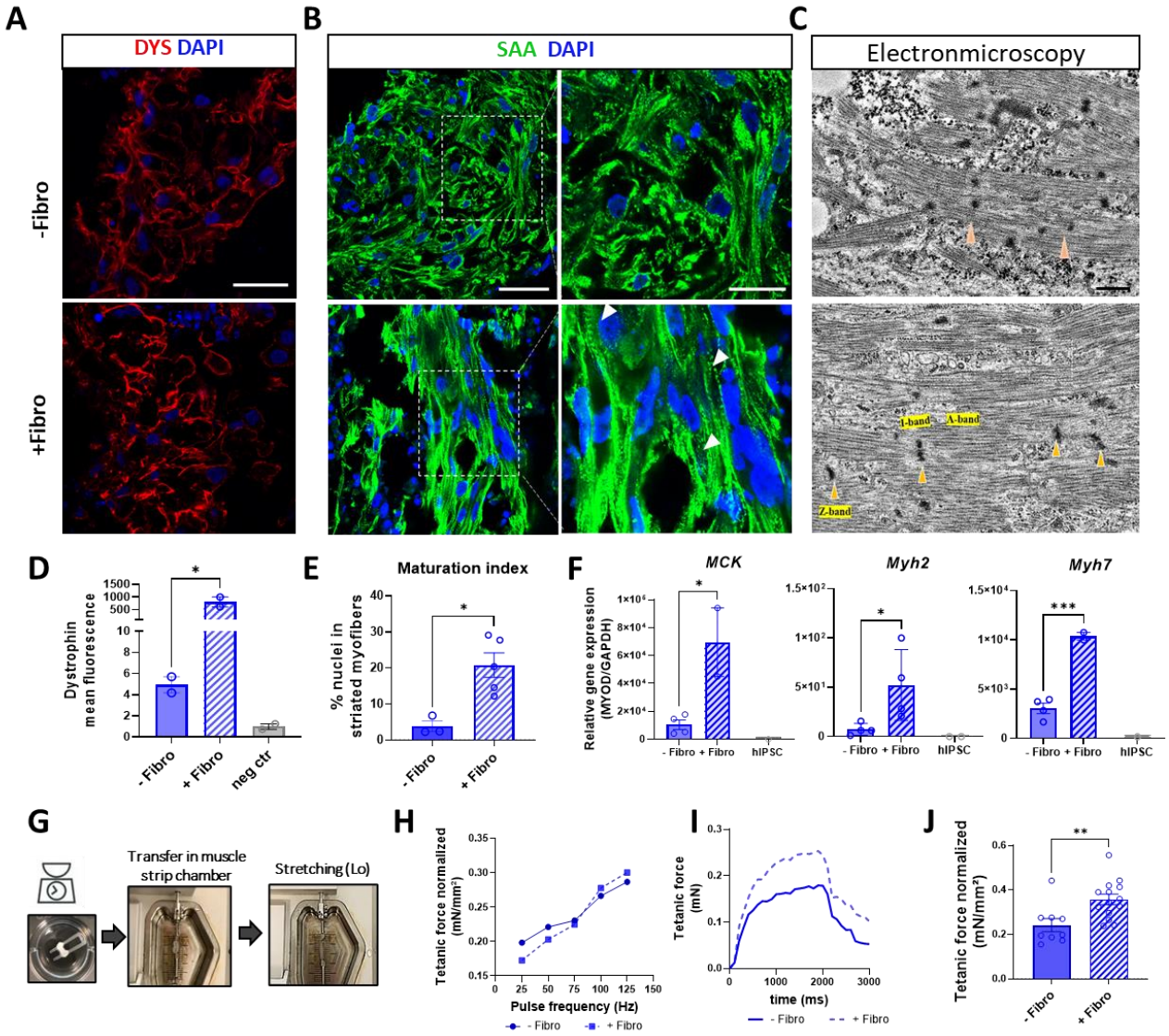

Figure 2. Structural and functional maturation in fibroblast-including MYOtissues. *(**A**) Representative transversal sections stained for Dystrophin. Scale bar: 40µm. Nuclei were visualized with DAPI **(B)** Representative longitudinal sections of MYOtissues +/- fibroblasts (fibro), immunostained for sarcomeric α-Actinin (SAA). Scale bars: 40µm, enlargement 10µm. (**C**) Transmission electron microscopy images showing sarcomeric structures. Orange arrows: Z-lines. Scale bar: 500nm. (**D**) Dystrophin staining quantification represented as mean intensity fluorescence and expressed as fold change to the negative control (sections stained without first antibody). (**E**) Quantification of maturation index calculated as % of nuclei inside striated myofibers visualized by SAA staining. (**F**) Gene expression analysis of MCK, Myh2 and Myh7, reported as gene expression relative to MYOD expressing population (**G**) Contractile muscle force analysis of MYOtissues using a muscle-strip based organ bath system. Before placement in the strip chamber, MYOtissues were weighted, and optimal length (Lo) measured for normalization of force data (see methods). (**H**) Normalized force-frequency relationships*

*in MYOtissues +/- fibro (n=2). (**I**) Representative tetanic force traces at optimal frequency (125 Hz) in MYOtissues +/- fibro. (**J**) Normalized tetanic force peak in MYOtissues +/- fibroblasts (n=8 to 15). Data are presented as means +/- SEM. Unpaired t test was applied for statistical analysis for maturation index (panel F) and for normalized tetanic force analysis (panel J). For all the other panels, One-way ANOVA statistical test was performed. (*p ≤0.05, **p ≤ 0.01, ***p ≤ 0.001, ****p ≤ 0.0001).*

857 **Figure 3**

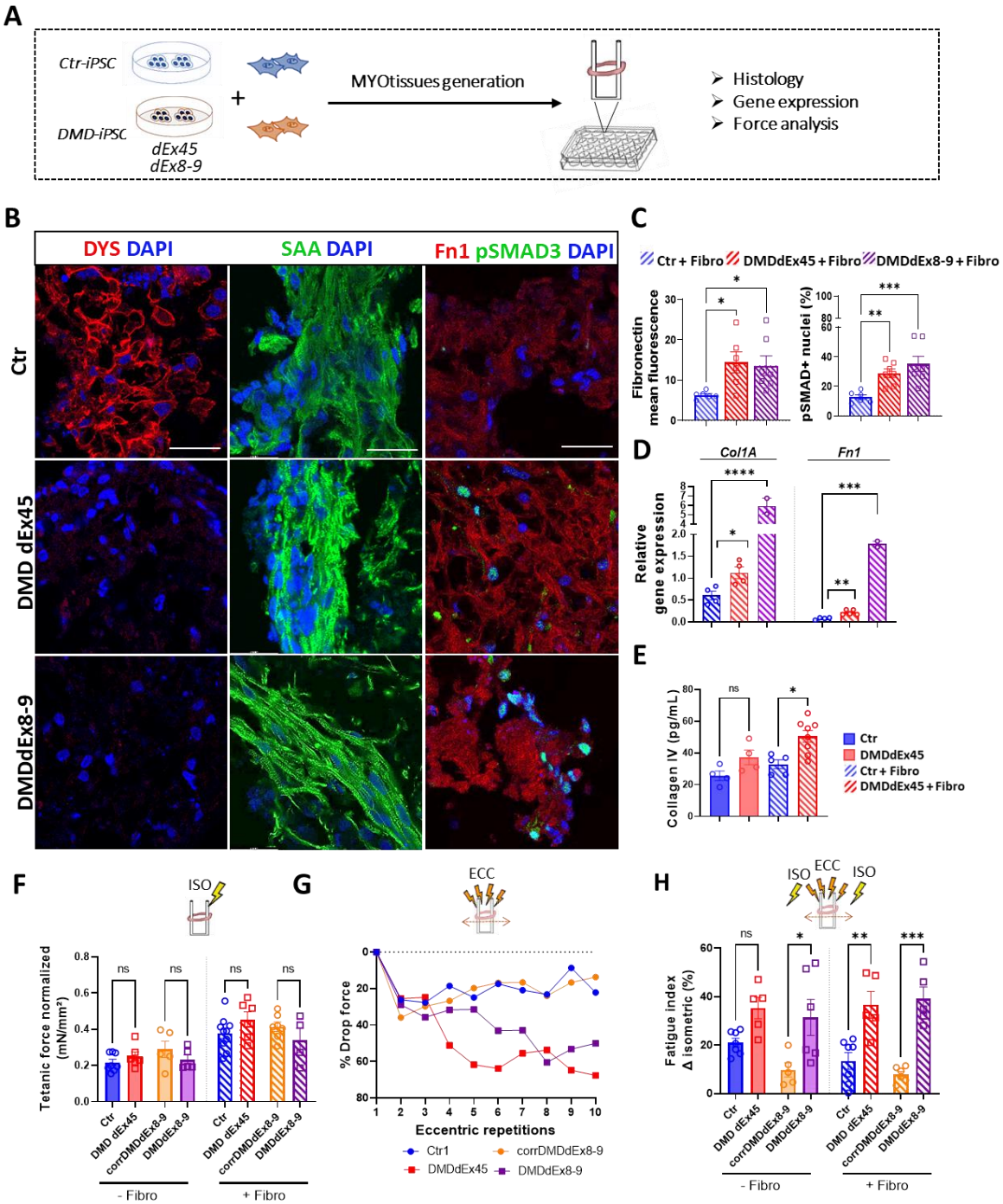

858

859 ***Figure 3. DMD iPSC-MYOtissues including DMD fibroblasts exacerbate pathogenic hallmarks. (A)*** *Overview*
860 *of MYOtissues generation from control (Ctr) and DMD iPSC (dEX45 and dEx8-9) including ctr or dystrophic*
861 *fibroblasts respectively for histological characterization and gene expression analysis.* ***(B)*** *Immunostaining of*
862 *MYOtissues cross sections for Dystrophin (Dys) or Fibronectin (Fn1)/pSMAD3 and for SAA in longitudinal*
863 *sections. Scale bar: 40µm.* ***(C)*** *Quantification of Fn1 signal and % of pSMAD3 nuclei in Ctr and DMD*
864 *MYOtissues.* ***(D)*** *RT-ddPCR analysis of fibrotic markers in Ctr or DMD iPSC-derived MYOtissues with*
865 *fibroblasts.* ***(E)*** *Expression level of Collagen IV secreted in Ctr and DMD MYOtissues with fibroblasts (f) and*

without fibroblasts. ***(F)*** *Isometric (ISO) contraction analysis: tetanic force developed normalized for CSA in Ctr, DMD and corrDMDdEx8-9 MYOtissues with and without fibroblasts* ***(G)*** *Force drop over 10 repetitions of eccentric (ECC) contractions in Ctr, DMD and corrDMDdEx8-9 MYOtissues including fibroblasts****(H)*** *Fatigue index, calculated as % of drop force between two ISO performed before and after 10x repetitions of* ECC *in Ctr, DMD and corrDMDdEx8-9 MYOtissues +/- respective fibroblasts. Data are presented as mean ± SEM (n=3-8). One-way ANOVA with Tukey's correction was performed for statistical purposes (*p ≤0.05, **p ≤ 0.01, ***p ≤ 0.001, ****p ≤ 0.000, ns= not significant*

875 **Figure 4**

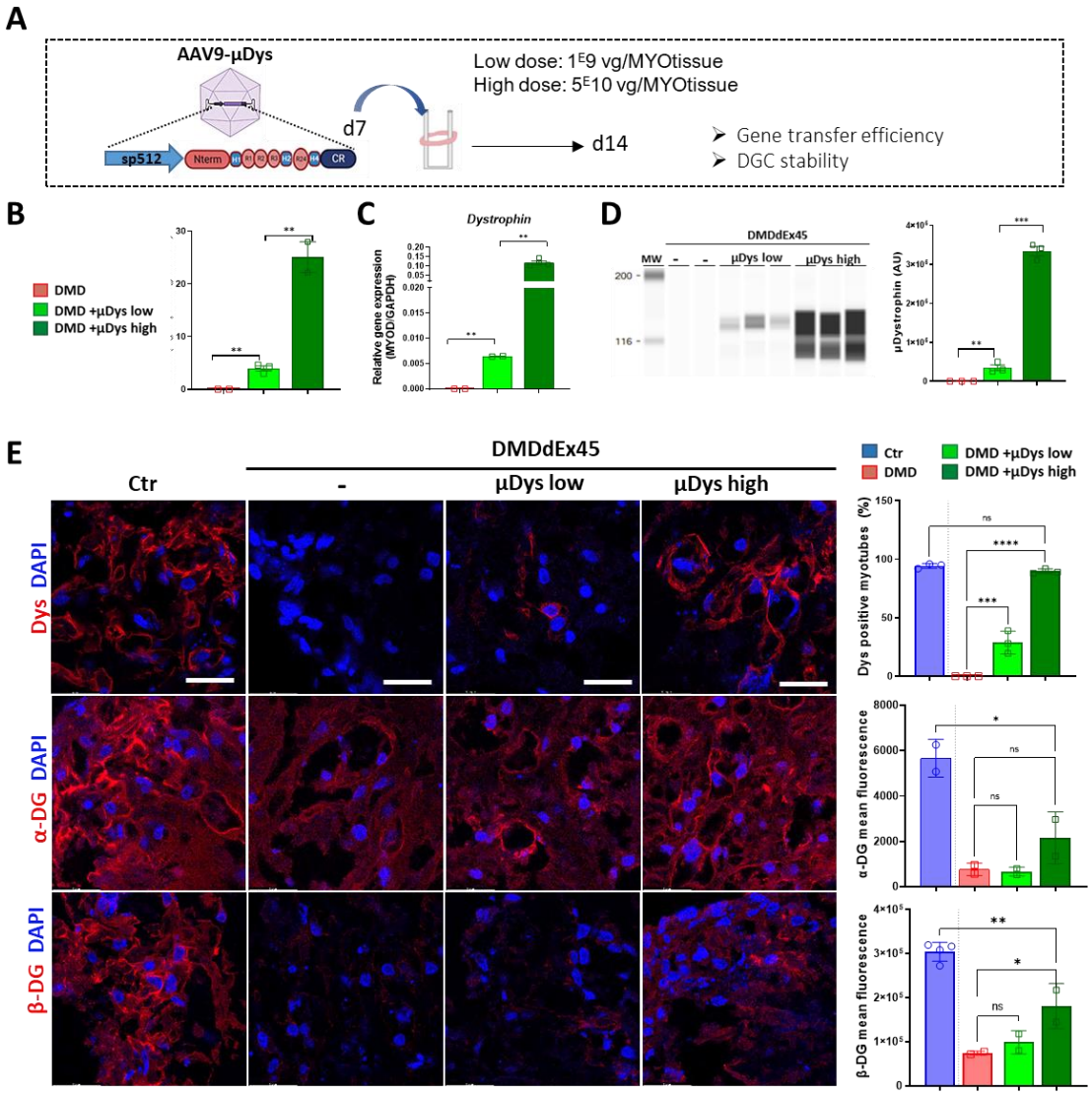

876

877 ***Figure 4. AAV-mediated delivery of µDys in exacerbated DMD MYOtissues ameliorates membrane stability***.
878 *(**A**) Scheme of AAV9-µDys infection and doses used in DMD iPSC-derived MYOtissues. (**B-C-D**) Evaluation of*
879 *gene transfer efficiency by Viral copy number (VCN) analysis **(B)**, mRNA expression levels **(C)** and protein*
880 *expression analysis by capillary western blot in DMD dEx45-derived MYOtissues infected with low and high*
881 *dose of µDys versus non infected (-), MW: molecular weight **(D)**. **(E)** Histological evaluation of Dystrophin*
882 *Glycoprotein Complex (DGC) upon infection, by immunostaining for Dystrophin (Dys), α-Dystroglycan (α-DG)*
883 *and β-Dystroglycan (β-DG) of WT and DMD cross sections of MYOtissues. Relative quantifications are shown.*
884 *Data are presented as means +/- SEM. Statistical analysis performed with one-way ANOVA analysis with*
885 *Tukey's correction (*p ≤0.05, **p ≤ 0.01, ***p ≤ 0.001, ****p ≤ 0.000, ns = not significant).*

886
887
888

Figure 5

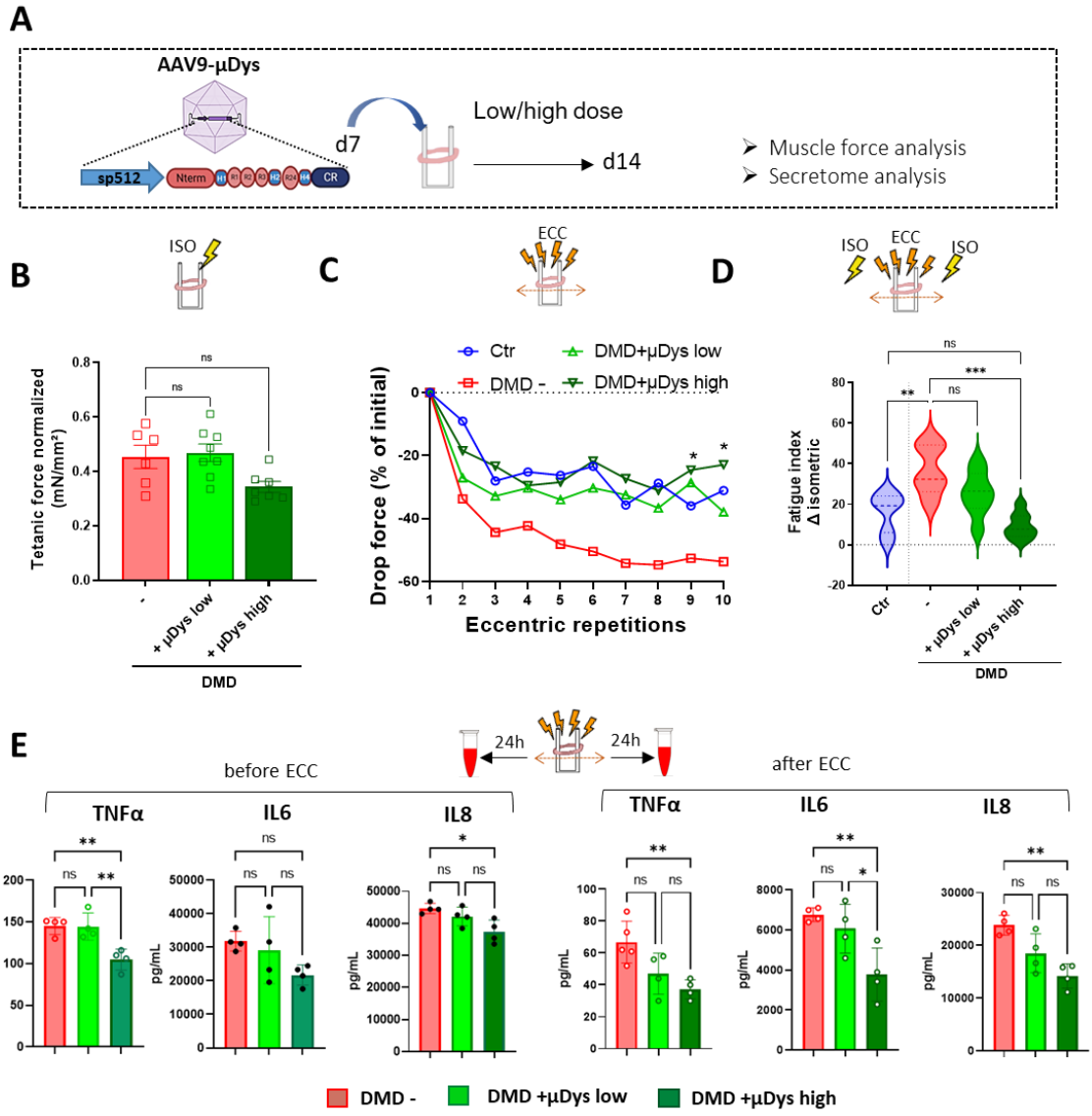

Figure 5. Muscle strength evaluation and secretome analysis following eccentric contractions. *(**A**) Ctr and DMDdEx45 MYOtissues subjected to muscle force assessment and to secretome analysis following AAV-µDys gene transfer. (**B**) Tetanic force normalized for cross section area (CSA) in untreated (-) and treated with µDystrophin (µDys) at low and high doses. **(C)** Drop force over 10 repetitions of eccentric (ECC) contractions in Ctr and DMDdEx45 MYOtissues including fibroblasts and treated with low and high dose of µDys. **(D)** Fatigue index in Ctr and DMDdEx45 MYOtissues treated or not with µDystrophin **(E)** Quantification of TNF alpha, IL-6 and IL-8 cytokines released in the media before and after the isometric and eccentric exercises. Data are presented as mean ± SEM (n=2-8) Statistical analysis performed with one-way ANOVA analysis with Tukey's correction (*p ≤0.05, **p ≤ 0.01, ***p ≤ 0.001) ns, not significant.*